Detection of Brain Activity for Averaged Multiple-Trial Magnetoencephalography Data

Yoshio Konno
Sophia University
7-1 Kioicho, Chiyoda-ku, Tokyo, Japan
yo-konno@sophia.ac.jp

Jianting Cao
Saitama Institute of Technology
1690 Fusaiji, Okabe, Saitama, Japan
Brain Signal Processing, RIKEN
2-1 Hirosawa, Wako-shi, Saitama, Japan

Takayuki Arai
Sophia University
7-1 Kioicho, Chiyoda-ku, Tokyo, Japan

Tsunehiro Takeda
Graduate School of Tokyo University
7-3-1 Hongo, Bunkyo-ku, Tokyo, Japan

Abstract

Treating averaged multiple-trial data is a common approach in recent papers for applying independent component analysis (ICA) to neurobiological signal processing. Although averaging increases the signal-to-noise ratio (SNR), important information is lost, such as the strength of an evoked response and its dynamics. Alternatively, when averaging few-trial data, not much information is lost, but SNR is very poor. In this paper, we deal with averaged data of few as well as of many trials, and we demonstrate that not only the location, but also the direction vector and dipole moment of evoked fields (EFs) can be obtained by applying our method, even when the number of trials is small.

1. Introduction

Many researchers have applied independent component analysis (ICA) to electroencephalographic (EEG) or magnetoencephalographic (MEG) data to determine the behavior and localization of brain sources [1, 2, 3, 4, 6]. However, because the magnetic field of brain signals is weak, spontaneous and environmental noise makes it difficult to recognize brain signals in recorded data.

The most widely used technique for reducing instrumental and environmental noises, and for identifying the behavior and location of activities of interest, such as evoked field responses, is to take an average across many stimulation trials. In fact, when applying ICA to MEG data, most researchers have treated averaged data [1, 2, 4]. However, by taking an average, important information is lost, making it advantageous to decrease the number of averages across data trials. The disadvantage of having fewer averages is that because SNR is very poor, the decomposition of a low-power source signal from recorded data is still influenced by noise. In this paper, we deal with small numbers of trials (averaged 10-trials) and large numbers of trials (averaged 100-trials), and we demonstrate that evoked signals can be detected by applying our ICA approach in both cases.

When applying ICA to physiological data, most researchers have used real, measured, physiological data, with some individual responses evoked by stimuli, and their decomposed components are evaluated from a neuroscience perspective. In this study, we use a synthesized MEG data set, which includes an artificial evoked field and real, measured brain data. The behavior of our data set is similar to auditory evoked fields (AEFs). The main advantage of our data set is that dipole location of evoked responses and its dynamics are known in advance, which facilitates the evaluation of the decomposed components. In this paper, to evaluate the results of decomposition, we focus on not only the location but also the direction vector and dipole moment of evoked fields.

2. Data analysis model

In this section, we describe the model for applying ICA to MEG data. Based on the principle of MEG measurement, this problem can be formulated as

$$\mathbf{x}(t) = \mathbf{A}\mathbf{s}(t) + \mathbf{e}(t), \tag{1}$$

where $\mathbf{x}(t)$, $\mathbf{s}(t)$ and $\mathbf{e}(t)$ represent the transpose of m observations at time t, n unknown source components and additive noise, respectively. Since neither human tissue nor

skull attenuate magnetic fields in MEG, $\mathbf{A}$ can be represented by a numerical matrix whose element a_{ij} is simply a quantity related to the physical distance between the i-th sensor and the j-th source.

In the model, $\mathbf{s}(t)$, $\mathbf{e}(t)$, $\mathbf{A}$ and n are unknown but $\mathbf{x}(t)$ are accessible. It is assumed that the components of $\mathbf{s}(t)$ are mutually statistically independent, as well as being statistically independent of the noise components $\mathbf{e}(t)$. Moreover, the noise components $\mathbf{e}(t)$ themselves are assumed to be mutually independent.

3. Data analysis method

3.1. Robust pre-whitening technique

In this subsection, we describe our robust pre-whitening technique [1, 2, 3]. This technique is very capable of reducing the power of additive noise.

When the sample size is sufficiently large, the covariance matrix of the observed data in the mixing model $\mathbf{\Sigma}$ can be written as $\mathbf{\Sigma} = \mathbf{A}\mathbf{A}^T + \mathbf{\Psi}$, where $\mathbf{\Psi}$ is a diagonal matrix of the additive noise $\mathbf{e}$. Also the covariance matrix of the observed data recorded by sensors can be given by $\mathbf{C} = \mathbf{x}\mathbf{x}^T$.

For the robust pre-whitening technique, $\mathbf{A}$ can be estimated as

$$\widehat{\mathbf{A}} = \mathbf{U}_{\hat{n}}\mathbf{\Lambda}_{\hat{n}}^{\frac{1}{2}}, \tag{2}$$

by applying the standard PCA approach, where $\mathbf{\Lambda}_{\hat{n}}$ is a diagonal matrix whose elements are eigenvalues of $\mathbf{C}$, the columns of $\mathbf{U}_{\hat{n}}$ are the corresponding eigenvectors and $\widehat{n}$ is the estimated number of sources.

To estimate $\mathbf{\Psi}$, we fit $\mathbf{\Sigma}$ to $\mathbf{C}$ using the eigenvalue decomposition method. In this case, the cost function is obtained as $L(\mathbf{A}, \mathbf{\Psi}) = tr[\mathbf{\Sigma} - \mathbf{C}]^2$. And we minimize it by $\frac{\partial L(\mathbf{A},\mathbf{\Psi})}{\partial \mathbf{\Psi}} = 0$, whereby the estimate noise variance $\mathbf{\Psi}$ is obtained as

$$\widehat{\mathbf{\Psi}} = diag(\mathbf{C} - \widehat{\mathbf{A}}\widehat{\mathbf{A}}^T), \tag{3}$$

where the estimate $\widehat{\mathbf{A}}$ is obtained in the same manner as shown in Eq. (2). Using these estimates $\widehat{\mathbf{A}}$ and $\widehat{\mathbf{\Psi}}$, we can obtain the transform matrix for the robust pre-whitening technique as

$$\mathbf{Q} = [\widehat{\mathbf{A}}^T\widehat{\mathbf{\Psi}}^{-1}\widehat{\mathbf{A}}]^{-1}\widehat{\mathbf{A}}^T\widehat{\mathbf{\Psi}}^{-1}. \tag{4}$$

Using the above result, the new set of data transformed from the observations can be obtained by

$$\mathbf{z}(t) = \mathbf{Q}\mathbf{x}(t). \tag{5}$$

Note that the covariance matrix is $E\{\mathbf{z}\mathbf{z}^T\} = \mathbf{I}_{\hat{n}} + \mathbf{Q}\mathbf{\Psi}\mathbf{Q}^T$, which implies that the source signals in a subspace are decorrelated.

A similar noise reduction approach that applies factor analysis (FA) to the decomposition of MEG data has been reported in [4]. Both this method and ours take additive noises into account, but with our robust pre-whitening technique, the distribution of additive noises is not restricted. Therefore, our technique is more robust and effective for data with non-Gaussian noise such as the outlier.

3.2. JADE algorithm

It should be noted that the robust pre-whitening technique is needed to reduce the power of sensor noises and the number of parameters, but it is insufficient to obtain the independent components since an orthogonal matrix in general contains additional degrees of freedom. Therefore, the remaining parameters must be further estimated by using an ICA algorithm. In this study, we apply the JADE altorithm [5].

The JADE algorithm has two procedures termed orthogonalization in PCA and rotation. We did apply the rotation procedure in the JADE algorithm, described below, but instead of the orthogonalization in PCA, we applied the robust pre-whitening technique described in Section **3.1**.

The rotation procedure in JADE uses matrices $\mathbf{F}(\mathbf{M})$ formulated by the fourth-order cumulant tensor of the outputs with an arbitrary matrix $\mathbf{M}$ as

$$\mathbf{F}(\mathbf{M}) = \sum_{k=1}^{K}\sum_{l=1}^{L} \mathrm{Cum}(z_i, z_j, z_k, z_l) m_{lk}, \tag{6}$$

where the $\mathrm{Cum}(\cdot)$ denotes a standard cumulant and m_{lk} is the (l,k)-th element of matrix $\mathbf{M}$. The correct rotation matrix $\mathbf{W}$ can be obtained by diagonalizing the matrix $\mathbf{F}(\mathbf{M})$, i.e. $\mathbf{W}\mathbf{F}(\mathbf{M})\mathbf{W}^T$ approximates a diagonal matrix.

After performing the robust pre-whitening technique and rotation in JADE, the de-mixture matrix is $\mathbf{WQ}$. With it, we can calculate the decomposed sources $\mathbf{y} \in \mathbf{R}^n$ as

$$\mathbf{y}(t) = \mathbf{W}\mathbf{z}(t) = \mathbf{W}\mathbf{Q}\mathbf{x}(t). \tag{7}$$

3.3. Power of decomposed components

The robust pre-whitening and ICA techniques serve to filter the raw data, decreasing the power of the additive noises and decomposing the sources. The estimated behavior of the individual sources can be represented as Eq. (7). To better visualize the information, we projected the decomposed components onto the sensor space.

The virtual sensor signals coming from multiple components are obtained as

$$\widehat{\mathbf{x}}(t) = \widehat{\mathbf{A}}\mathbf{W}^{-1}\mathbf{y}(t). \tag{8}$$

To determine the information of the k-th individual components, we forced every element to be zero except the k-th

Table 1. Artificial evoked fields.

	peak time (sec.)	location x, y, z (mm)	vector az, dec (deg.)	moment Q (nAm)
Evoked Field 1	0.25	10, 50, 50	150, 108	20
Evoked Field 2	0.27	-40, 40, 40	250, 59	30

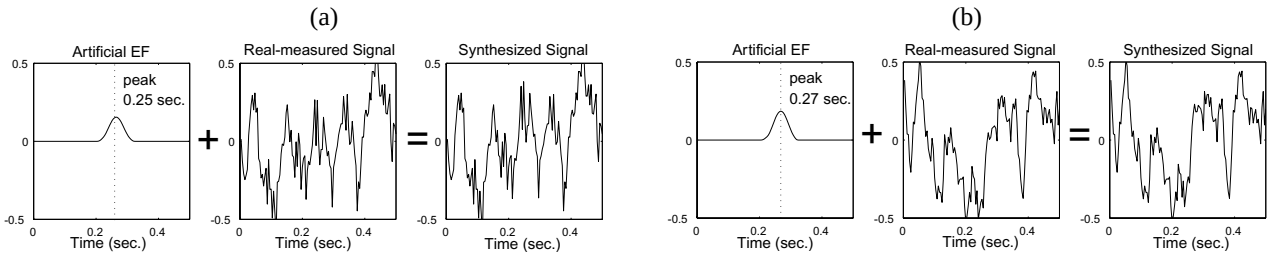

Figure 1. An example for data synthesizing: (a) Data synthesizing at sensor-L24, which detects signal EF1. (b) Data synthesizing at sensor-L44, which detects signal EF2. In each example, artificial EF signals (left), real measured MEG signals (middle), synthesized signals (right) are represented. The horizontal axis expresses time (sec.) and the vertical axis expresses amplitude (pT).

$(k = 1, \cdots, \widehat{n})$ of $\mathbf{y}(t)$ in Eq. (8). The virtual sensor signals coming from k-th individual components are obtained as

$$\widehat{\mathbf{x}}_k(t) = \widehat{\mathbf{A}}\mathbf{W}^{-1}[0 \cdots \mathbf{y}_k(t) \cdots 0]^T. \tag{9}$$

The relationship between virtual sensor signals from multiple $\widehat{\mathbf{x}}$ and k-th individual components $\widehat{\mathbf{x}}_k$ is $\widehat{\mathbf{x}}(t) = \sum_{k=1}^{\hat{n}} \widehat{\mathbf{x}}_k(t)$. Note that some noises have been reduced in the estimated observation $\widehat{\mathbf{x}}_k(t)$.

In this paper, we define the total sum of each virtual sensor signal from the k-th individual component as:

$$\mathbf{v}_k(t) = \frac{1}{M} \sum_{i=1}^{M} \widehat{\mathbf{x}}_{k,i}(t) \tag{10}$$

to compare the power of decomposed components. In Eq. (10), M denotes the number of sensors and $\widehat{\mathbf{x}}_{k,i}$ denotes the k-th decomposed components of $\mathbf{y}(t)$ into the i-th sensor. Here $\mathbf{v}_k$ represents the total observation signals derived by the k-th decomposed signal, so that its amplitude is not ambiguous.

Using the above results, we define the power of the k-th decomposed components $\mathbf{v}_k$ as

$$P_{\mathbf{v}k} = \sum_{t=1}^{N} \mathbf{v}_k(t)\mathbf{v}_k^T(t), \tag{11}$$

where, N denotes the number of data samples. Applying $P_{\mathbf{v}k}$ as the power of the k-th decomposed components, we can compare the power of individual components decomposed by ICA.

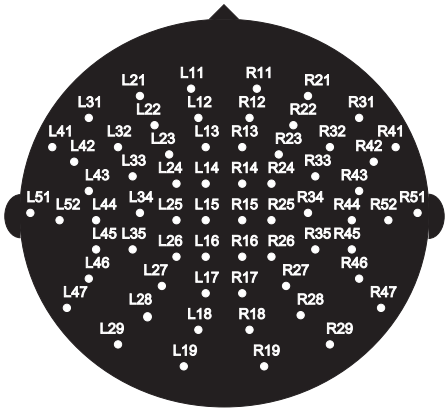

Figure 2. Sensor distribution.

4. Experimental results

4.1. Synthesized MEG data

In this subsection, we describe the synthesized MEG data set, used for simulation, which is similar to Auditory Evoked Fields (AEFs). As shown in Fig. 1, we synthesized an artificial signal and a real measured MEG signal which is recorded by using an Omega-64 (CTF Systems Inc., Canada). The sensor arrays consist of 64 channels and the sensor distribution is shown in Fig. 2. The sampling rate was 250 Hz with duration of 50 sec. for 12500 samples. The observed data $\mathbf{X}_{(64\times12500)}$ was segmented into 100 trials, so the duration of each trial $\mathbf{X}_{i(64\times125)}(i = 1, \cdots, 100)$ is 0.5 sec. and each trial has 125 samples, where i denotes the trial number.

The source signals in this data set include two different

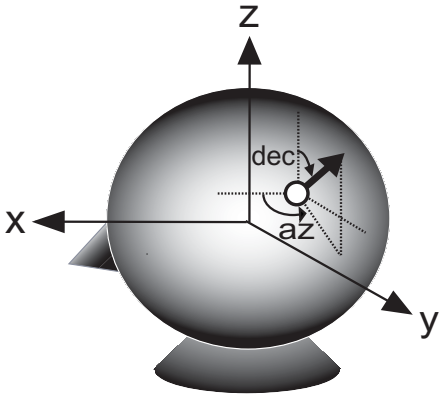

Figure 3. 3D frames of reference.

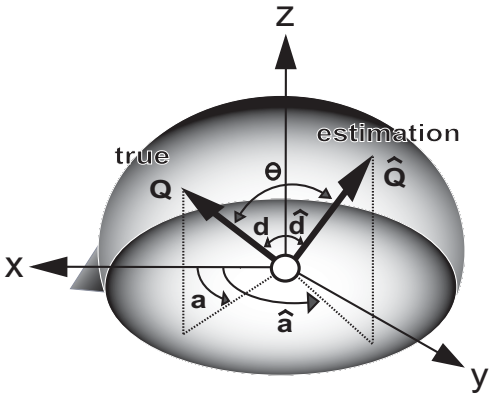

Figure 4. Angle Θ between the direction vector of true and estimated EFs, in case of uniting the starting point of two vectors (a : azimuth, d : declination).

evoked fields responses, EF1 and EF2, and include the 50 Hz electrical power interference and the α-wave component involved in the real measured MEG data. The signal EF1 was artificially evoked from 0.2 sec. to 0.3 sec. with a peak at 0.25 sec. and its strength (dipole moment) was $Q = 20$ nAm (see Fig. 1(a)). The signal EF2 was artificially evoked from 0.22 sec. to 0.32 sec. with a peak at 0.27 sec. and its strength was $Q = 30$ nAm (see Fig. 1(b)). The source of EF1 was located at $[x,\ y,\ z] = [10,\ 50,\ 50]$ mm and that of EF2 was located at $[x,\ y,\ z] = [-40,\ 40,\ 40]$ mm, where a head model presupposes a sphere with a radius of 75 mm and x, y, z axis are set according to Fig. 3. The direction vector, azimuth (az) and declination (dec), of EF1 was set at $[az,\ dec] = [150,\ 108]$ deg. and that of EF2 was set at $[az,\ dec] = [250,\ 59]$ deg. (see Table 1).

4.2. Automatic classification

In this subsection, we demonstrate the procedure for automatic classification of the decomposed components into signals EF1 and EF2. First, we calculated the power of each decomposed component in the time domain

$$P_{\mathbf{v}k} = \sum_{t=0}^{0.5} \mathbf{v}_k(t)\mathbf{v}_k^T(t), \tag{12}$$

where $\mathbf{v}_k(t)$ denotes the k-th decomposed component. To define the criterion for classifying the decomposed components into EF1 and EF2, we calculated the power of each decomposed component in the duration from 0.2 to 0.3 sec. $P'_{\mathbf{v}k}$ and from 0.22 to 0.32 sec. $P''_{\mathbf{v}k}$ as

$$P'_{\mathbf{v}k} = \sum_{t=0.2}^{0.3} \mathbf{v}_k(t)\mathbf{v}_k^T(t),$$
$$P''_{\mathbf{v}k} = \sum_{t=0.22}^{0.32} \mathbf{v}_k(t)\mathbf{v}_k^T(t). \tag{13}$$

Using above results, we define the ratios

$$R'_{\mathbf{v}k} = \frac{P'_{\mathbf{v}k}}{P_{\mathbf{v}k}}, \quad R''_{\mathbf{v}k} = \frac{P''_{\mathbf{v}k}}{P_{\mathbf{v}k}}. \tag{14}$$

When $R'_{\mathbf{v}k} \geq k_{EF1}$, the decomposed component $\mathbf{v}_k$ is the signal EF1, since the signal EF1 was artificially evoked from 0.2 to 0.3 sec., where k_{EF1} is a positive constant. Similarly, when $R''_{\mathbf{v}k} \geq k_{EF2}$, the decomposed component $\mathbf{v}_k$ is the signal EF2, where k_{EF2} is a positive constant. Based on prior experience, for this experiment we set these parameters as $k_{EF1} = 0.6$, $k_{EF2} = 0.6$, respectively [2].

4.3. Evaluation methods

In this study, since the dipole locations, direction vectors and dipole moments of EF1 and EF2 were known in advance, we can compare them to the estimated ones. We used the standard spatio-temporal dipole fitting routine, MEG v3.3a (CTF System Inc., Canada), to find the dipole. Here we define the distance between true dipole location $[x,\ y,\ z]$ mm and estimated dipole location $[\widehat{x},\ \widehat{y},\ \widehat{z}]$ mm as

$$r = \sqrt{(x-\widehat{x})^2 + (y-\widehat{y})^2 + (z-\widehat{z})^2}. \tag{15}$$

When uniting the starting point of two vectors, we define the angle Θ between the direction vector of true and estimated EFs as

$$\Theta = \cos^{-1}[\sin(d)\sin(\widehat{d})\cos(a-\widehat{a}) + \cos(d)\cos(\widehat{d})], \tag{16}$$

where a and d denote azimuth and declination (deg.), respectively (see Fig. 4). We define the difference of true and estimated dipole moment ΔQ as

$$\Delta Q = |Q - \widehat{Q}|, \tag{17}$$

where Q and $\widehat{Q}$ denote the dipole moments (nAm) of the EFs and their estimates, respectively.

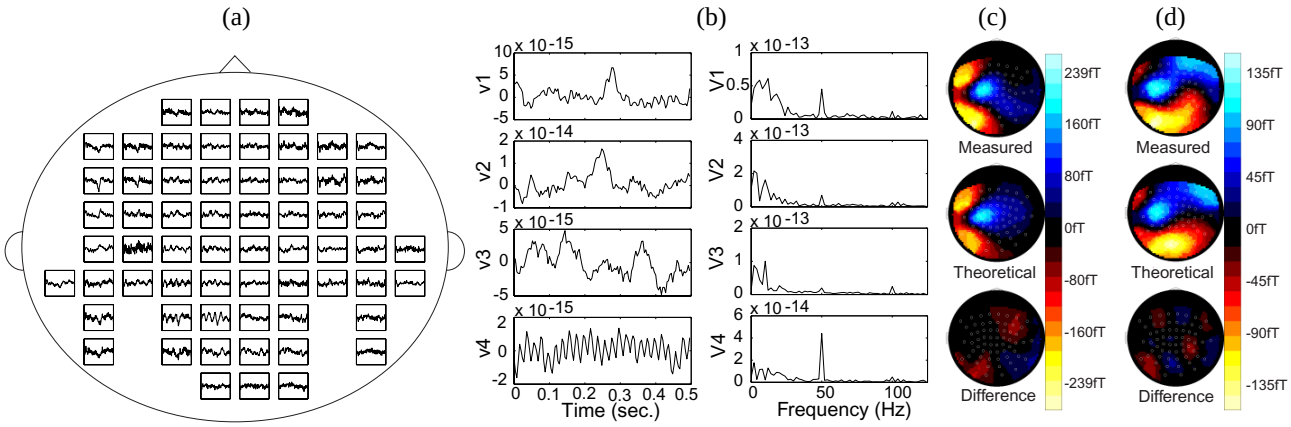

Figure 5. (a) Averaged of 10 trials data. (b) Result of ICA with the robust pre-whitening technique and its frequency contents. (c) Estimated map focus on EF1, (d) Estimated map focus on EF2.

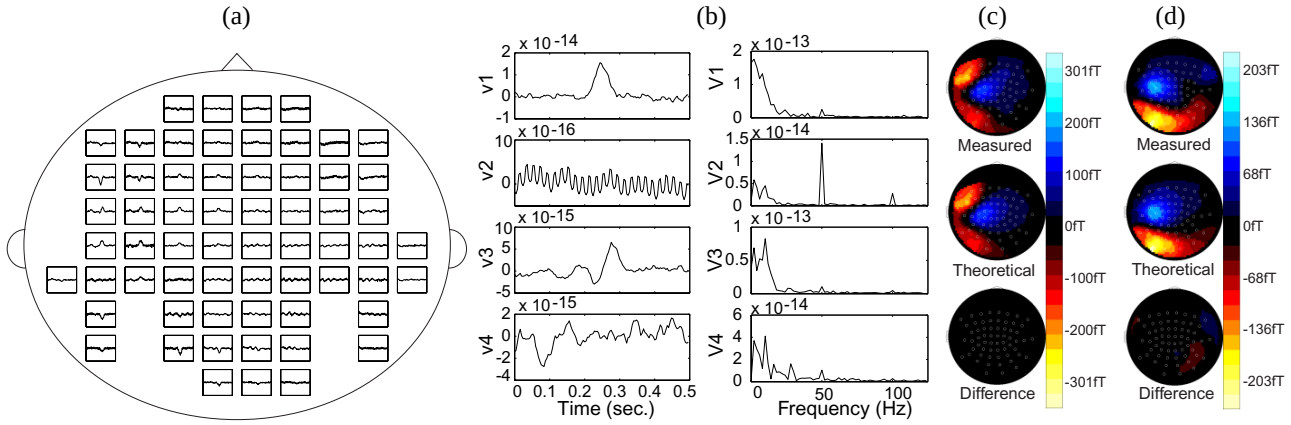

Figure 6. (a) Averaged of 100 trials data. (b) Result of ICA with the robust pre-whitening technique and its frequency contents. (c) Estimated map focus on EF1, (d) Estimated map focus on EF2.

4.4. Results for averaged 10-trials data

We demonstrate the results for the averaged 10-trial data, as shown in Fig. 5(a). In this figure, the horizontal axis and vertical axis express time from 0 to 0.5 sec. and amplitude from -0.5 to 0.5 pT, respectively. The results $\mathbf{v}(t)$ and these power spectrums $\mathbf{V}_k(f)$ are shown in Fig. 5(b). Applying the automatic classifying technique described in Sect. 4.2, $\mathbf{v}_1$ and $\mathbf{v}_2$ have satisfied the equations $R''_{\mathbf{v}1} \geq k_{EF2}$ and $R'_{\mathbf{v}2} \geq k_{EF1}$, respectively, and can thus be regarded as signals EF2, EF1, respectively.

The estimated maps of signals EF1 and EF2, derived by analyzing the average of 10-trials (after ICA), are shown in Fig. 5(c)(d), respectively. As for the result of EF1, note that the evoked response appears on the left-front area of the brain. For the result of EF2, the evoked response appears on the left-back area of the brain. The results of dipole estimation become $[\widehat{x},\ \widehat{y},\ \widehat{z}] = [-5.7,\ 46.4,\ 47.5]$ mm, $[\widehat{az},\ \widehat{dec}] = [145.1,\ 123.3]$ deg. and $\widehat{Q} = 50.0$ nAm for EF1 and $[\widehat{x},\ \widehat{y},\ \widehat{z}] = [-37.5,\ 24.1,\ 52.9]$ mm, $[\widehat{az},\ \widehat{dec}] = [293.6,\ 55.0]$ deg. and $\widehat{Q} = 30.6$ nAm for EF2. Using Eq. (15), (16) and (17), the difference between true and estimated dipole, r, Θ and ΔQ are $r = 16.3$ mm, $\Theta = 15.9$ deg. and $\Delta Q = 30.0$ nAm for EF1 and $r = 20.6$ mm, $\Theta = 36.5$ deg. and $\Delta Q = 0.6$ nAm for EF2, respectively (see Table 2).

Here, we describe the results of dipole estimation for averaged 10-trials data (before ICA). The results of dipole estimation for averaged 10-trials data become $[\widehat{x},\ \widehat{y},\ \widehat{z}] = [7.8,\ 16.5,\ 46.4]$ mm, $[\widehat{az},\ \widehat{dec}] = [167.2,\ 85.1]$ deg. and $\widehat{Q} = 119.8$ nAm for EF1 and $[\widehat{x},\ \widehat{y},\ \widehat{z}] = [-38.2,\ 12.5,\ 52.3]$ mm, $[\widehat{az},\ \widehat{dec}] = [299.8,\ 60.4]$ deg. and $\widehat{Q} = 41.1$ nAm for EF2. Therefore r, Θ and ΔQ are $r = 33.8$ mm, $\Theta = 28.5$ deg. and $\Delta Q = 99.8$ nAm for EF1 and $r = 30.2$ mm, $\Theta = 42.7$ deg. and $\Delta Q = 11.1$ nAm for EF2, respectively. The results show that by applying our ICA approach, we can obtain more accurate information about EFs.

Table 2. Comparison of true and estimated EFs

(a) Estimation of EF1.

		dipole location (mm)				direction vector (deg.)			moment (nAm)	
		x	y	z	r	az	dec	Θ	Q	ΔQ
true value		10.0	50.0	50.0	-	150.0	108.0	-	20.0	-
averaged 10-trials	after ICA	-5.7	46.4	47.5	16.3	145.1	123.3	15.9	50.0	30.0
	before ICA	7.8	16.5	46.4	33.8	167.2	85.1	28.5	119.8	99.8
averaged 100-trials	after ICA	8.9	47.0	50.9	3.4	149.5	107.6	0.6	24.3	4.3
	before ICA	5.6	57.3	48.1	8.7	141.5	123.0	16.8	13.4	6.6

(b) Estimation of EF2.

		dipole location (mm)				direction vector (deg.)			moment (nAm)	
		x	y	z	r	az	dec	Θ	Q	ΔQ
true value		-40.0	40.0	40.0	-	250.0	59.0	-	30.0	-
averaged 10-trials	after ICA	-37.5	24.1	52.9	20.6	293.6	55.0	36.5	30.6	0.6
	before ICA	-38.2	12.5	52.3	30.2	299.8	60.4	42.7	41.1	11.1
averaged 100-trials	after ICA	-37.1	37.0	36.3	5.6	259.6	50.7	11.4	33.0	3.0
	before ICA	-43.0	37.5	44.4	5.9	245.1	70.3	12.1	33.4	3.4

4.5. Results for averaged 100-trials data

Next, we describe the results of averaged 100-trials data, as shown in Fig. 6(a). The results $\mathbf{v}(t)$ and these power spectrums $\mathbf{V}_k(f)$ are shown in Fig. 6(b). Here, $\mathbf{v}_1$ and $\mathbf{v}_3$ have satisfied the equation $R'_{\mathbf{v}1} \geq k_{EF1}$ and $R''_{\mathbf{v}3} \geq k_{EF2}$, respectively, and can thus be regarded as EF1 and EF2, respectively.

The estimated maps of the EF1 and EF2 derived by analyzing the averaged 100-trials data (after ICA) are shown in Fig. 6(c)(d), respectively. In the results of EF1 and EF2, note that the evoked responses appear like the maps derived by analyzing the averaged 10-trials data. The results of dipole estimation are $[\widehat{x},\ \widehat{y},\ \widehat{z}] = [8.9,\ 47.0,\ 50.9]$ mm, $[\widehat{az},\ \widehat{dec}] = [149.5,\ 107.6]$ deg. and $\widehat{Q} = 24.3$ nAm at EF1 and $[\widehat{x},\ \widehat{y},\ \widehat{z}] = [-37.1,\ 37.0,\ 36.3]$ mm, $[\widehat{az},\ \widehat{dec}] = [259.6,\ 50.7]$ deg. and $\widehat{Q} = 33.0$ nAm at EF2. Therefore r, Θ and ΔQ are $r = 3.4$ mm, $\Theta = 0.6$ deg. and $\Delta Q = 4.3$ nAm for EF1 and $r = 5.6$ mm, $\Theta = 11.4$ deg. and $\Delta Q = 3.0$ nAm for EF2 (see Table 2).

The results of dipole estimation for averaged 100-trials data (before ICA) become $[\widehat{x},\ \widehat{y},\ \widehat{z}] = [5.6,\ 57.3,\ 48.1]$ mm, $[\widehat{az},\ \widehat{dec}] = [141.5,\ 123.0]$ deg. and $\widehat{Q} = 13.4$ nAm for EF1 and $[\widehat{x},\ \widehat{y},\ \widehat{z}] = [-43.0,\ 37.5,\ 44.4]$ mm, $[\widehat{az},\ \widehat{dec}] = [245.1,\ 70.3]$ deg. and $\widehat{Q} = 33.4$ nAm for EF2. Therefore r, Θ and ΔQ are $r = 8.7$ mm, $\Theta = 16.8$ deg. and $\Delta Q = 6.6$ nAm for EF1 and $r = 5.9$ mm, $\Theta = 12.1$ deg. and $\Delta Q = 3.4$ nAm for EF2.

Comparing the results of ICA and taking averages (before ICA), we conclude that not only dipole location, but also direction vector and dipole moment become more accurate by applying our ICA approach (see Table 2).

5. Conclusions

In this paper, we performed source decomposition of averaged multiple-trials MEG data using our ICA algorithm. Our results showed that the analysis of averaged data effectively determines not only dipole location but also direction vector and dipole moment of the evoked fields even when the number of averages is small. The authors hope these results will help neuroscientists to further their understanding of the temporal cortex.

References

[1] Y. Konno, J. Cao and T. Takeda, "Decomposition and Localization of MEG Brain Sources," Journal of Signal Processing, Vol. 6, No, 6, pp. 391-400, Nov 2002.

[2] Y. Konno, J. Cao, T. Arai and T. Takeda, "Visualization of Brain Activities of Single-Trial and Averaged Multiple-Trials MEG Data," IEICE Trans. on Fundamentals, Vol. E86-A, No. 9, pp. 2294-2302, Sep 2003.

[3] J. Cao, N. Murata, S. Amari, A. Cichocki and T. Takeda, "A robust approach to independent component analysis of signals with high-level noise measurements," IEEE Trans. on Neural Networks, Vol. 14, No. 3, pp. 631-645, June 2003.

[4] S. Ikeda, K. Toyama, "Independent component analysis for noisy data - MEG data analysis," Neural Networks 13, pp. 1063-1074, 2000.

[5] J. F. Cardoso and A. Souloumiac, "Jacobi angles for simultaneous diagonalization," SIAM J. Mat. Anal. Appl., Vol. 17, No. 1, pp. 145-151, 1996. Matlab code in WWW : http://sig.enst.fr/ cardoso/jointdiag.html

[6] Vigario, R., Sarela, J., Jousmiki, V., Hamalainen, M. and Oja, E, "Independent component approach to the analysis of EEG and MEG recordings," Biomedical Engineering, IEEE Transactions on, Vol. 47 Issue. 5, pp. 589-593, May 2000